
Article:
Li, X. and Dwyer-Joyce, R.S. orcid.org/0000-0001-8481-2708 (2020) Measuring friction at an interface using ultrasonic response. Proceedings of the Royal Society A: Mathematical, Physical and Engineering Sciences, 476 (2241). 20200283. ISSN 1364-5021

https://doi.org/10.1098/rspa.2020.0283

Measuring Friction at an Interface Using Ultrasonic Response

X. Li and R.S. Dwyer-Joyce

Leonardo Centre for Tribology, The University of Sheffield, Sheffield, UK

Abstract

Friction between sliding surfaces is a fundamental phenomenon prevalent in many aspects of engineering. There are many sliding contact tribometers that measure friction force in a laboratory environment. However, the transfer of laboratory data to real machine elements is unreliable. Results depend on the specimen configuration, surface condition and environment.

In this work a method has been developed that uses the nonlinear response of a high-power ultrasonic wave to deduce friction coefficient in-situ at an interface. When the high-power shear wave strikes a frictional interface, relative slip can occur. It imposes a nonlinear response and causes generation of higher-order odd frequency components in received ultrasonic signals. The amplitude of the harmonics depends on contact stress and local friction coefficient.

This nonlinear ultrasonic response has been investigated both numerically and experimentally. A simple 1D model has been used to predict nonlinearity generation. This model has been compared with experiments conducted on aluminium rough surfaces pressed together under increasing loads. Two strategies have been used to estimate the friction coefficient by correlating experimental and numerical third-order nonlinearity. It has proved possible to determine the friction coefficient in-situ at the interface; values in the range of 0.22 to 0.61 were measured for different surface configurations.

Key words: contact, friction, stick-slip, shear wave, contact acoustic nonlinearity

1 Introduction

Friction is present wherever one surface slides over another. It is a fundamental parameter that affects machine performance and operation. Despite this, measuring friction, and especially transferring results from the laboratory to real components, remains problematic. Measured friction depends strongly on the test specimen configuration, the environment, and critically on the surface preparation. The unifying feature of laboratory friction measuring devices is to measure the tangential force simultaneously with the normal force. The pin-on-disc specimen configuration, where a pin is held stationary and pressed against a rotating disc, and its variations are common means for macroscopic friction measurement. Friction force oscillation was commonly observed in this test, resulted from nonuniform condition on the disc due to lubrication and material transfer, and friction coefficient of dry sliding contact was reported of 0.31 with 17% error [1]. Atomic Force Microscopes (AFM) or its modification Friction Force Microscopes (FFM) are widely used to measure friction at the atomic scale in the field of micro-tribology [2]; the small friction force is determined by measuring the motion of a cantilever electronically or optically in the interaction of a sharp tip and the specimen surface. The normal force can be converted from vertical deflection of the cantilever and friction can be measured from the lateral deflection or twist of the cantilever. Experimental conditions of the AFM/FFM contribute in variations of measurement of friction force and friction coefficient and calibration methods are required and deviation of friction measurement varies from 5% [3] to 40% [4]. In both configurations, most measurement is taken during sliding and the kinetic friction coefficient is determined. The Centrifugal Friction Apparatus (CFA) is devised to measure the static friction [5], where a mass is placed on a rotating disc, in equilibrium by centrifugal force and friction. At the point the mass starts to slide, the centrifugal force is measured as the friction. Static friction coefficient of sliding samples were measured from 1.8 (38% deviation) to 0.36 (less than 5% deviation) with increased normal loads [5]. AFM was applied in measuring static friction coefficient and deviation was from 12% to 33% [6]. Factors affecting frictional behaviour limit the application of friction coefficient measured using these methods in physical situations [7]. An alternative approach is to measure the friction directly in a machine element, such as a bearing or gear pair. This is commonly achieved by measuring torque on the whole component, or subsystem, using some strain gauge based approach. This has the advantage of giving data for the real component in its natural operating environment. For example, thread friction in aerospace fasteners have been measured using this method and friction coefficient was 0.12 (approx.10% error) [8]. However, friction frequently originates at a number of contact interfaces in the component or sub-system that are under varying loads, and extracting friction coefficient for a particular interface is difficult.

In this work, rather than generating slip by macro-sliding, an ultrasonic pulse is used to generate nano-scale slip at an interface. We investigate ultrasound both to cause the relative sliding motion and to measure the resulting signal. Non-invasive ultrasonic methods have been extensively used in tribological systems to measure oil film thickness [9], lubricant viscosity [10] and contact pressure [11] in-situ. In these conventional ultrasonic techniques, pulses are low power and when they strike an interface they do not result in any irreversible change in the contact state. Deformations are small, and the process is linear and elastic. However, high power sound waves

can cause opening or closing of an interface [12], or interfacial slip [13]. This is non-linear and known as Contact Acoustic Nonlinearity (CAN). When a high power longitudinal polarised wave travels to a closed interface, it may open under tensile pressure or be further compressed under compressive pressure; this is known as the clapping effect. Ultrasound only propagates through the interface under compression and this discontinuity results in higher order harmonics (*2f, 3f*, etc.) being generated. Previous work has been based around CAN in longitudinal waves to investigate nonlinearity generation at un-bonded interfaces [12, 14, 15] and kissing bonds in adhesive joints [16].

When high power bulk shear ultrasound propagates through a compressed rough interface, its polarisation direction parallel to the interface, the shear stress induced may make the interface slip and cause a discontinuity. Higher odd order harmonics (*3f*, *5f*, etc.) are generated in both transmitted and reflected waves [17]. On the contrary to longitudinal waves, where stress causes interface clapping, a shear wave can trigger nonlinear stick-slip phenomena, and this nonlinearity generation may be useful in determining friction and friction coefficient [17, 18]. Previous studies [17-22] have focused on analytical and numerical studies of the ultrasonic nonlinearity at a contact interface. Contact nonlinearity generation at an interface caused by stick-slip phenomena using only normal incident shear waves has been studied using various approaches [17-21]. Blanloeuil et al. [22] focuses on oblique incident shear wave where both clapping and slipping effects can occur with the former being more dominant. Less common are studies of shear wave CAN by experiment; one particular example of which is the combined experimental and numerical approach of [21].

This work demonstrates how these principles of CAN in bulk shear waves can be used to estimate friction coefficient. The paper consists of three parts. Firstly, a simple numerical model is employed to investigate the harmonic generation from nonlinear interfacial stick-slip motion. The effects of incident wave amplitude, contact stress, and friction coefficient are studied. In the second part, nonlinearity generation is investigated experimentally using a high frequency nonlinear ultrasonic technique. The nonlinearity from the rough interface is assessed for various contact loading conditions. In the third part, the two approaches are combined to estimate the friction coefficient at a contact.

2 Nonlinear ultrasonic response from a frictional interface

The interaction of shear polarised ultrasound with a frictional interface is depicted schematically in Figure 1. Two identical homogeneous, isotropic elastic materials, *I* (defined by $x < 0$) and *II* ($x > 0$) are contacting under a normal contact stress, σ. At the interface ($x = 0$), friction is characterised by Coulomb's law with a constant friction coefficient, μ. When sliding the frictional shear stress is proportional to the applied normal contact stress ($\tau = \mu\sigma$). When a high-power shear polarised ultrasound strikes a frictional interface, interfacial slip distorts the wave. The ultrasonic wave generates a sinusoidally varying shear stress at the interface. When the peak amplitude of the wave exceeds the limiting frictional shear stress ($\tau = \mu\sigma$), the maximum tangential stress propagating through the interface is truncated to that limiting shear stress. The

Deleted:

stress waveform of the transmitted wave is therefore clipped and the reflected wave is distorted [17, 20], see also Figure 2 which is described later.

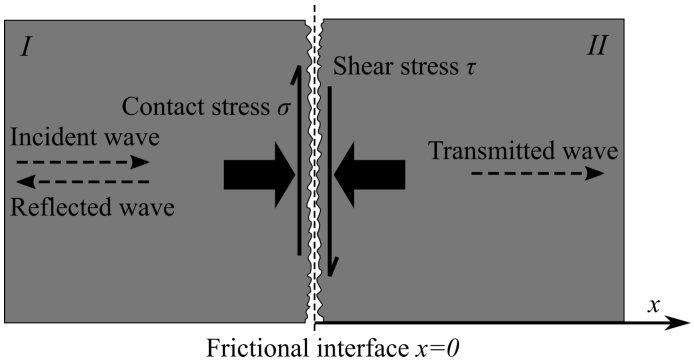

Figure 1 Schematic diagram of shear ultrasound incident at a normally rough interface.

A pure sinusoidal waveform is used as the incident wave because it consists of a single frequency and any distortion of reflected and transmitted waves can be examined for harmonic generation. The displacement and stress of the incident wave are given by [17, 21]:

$$f(x,t) = A_0\, sin(\omega t - kx), \tag{1}$$

$$\tau(x,t) = GkA_0\, cos(\omega t - kx), \tag{2}$$

where A_0, ω and k are the displacement amplitude, angular frequency and wavenumber of the shear ultrasonic wave, respectively. G is the shear modulus of the contacting material I and II.

At $t = 0$ the shear stress by ultrasound τ is greater than the limiting frictional stress $\mu\sigma$, and contact is assumed to be in 'slip' state. 'Slip' stops and 'stick' occurs at a critical time t_c when:

$$GkA_0|cos(\omega t_c)| = \mu\sigma. \tag{3}$$

Rearranging Equation (3) gives:

$$t_c = cos^{-1}\left(\frac{\mu\sigma}{GkA_0}\right). \tag{4}$$

When the shear stress overcomes the limiting friction, contact switches to 'slip' again. As depicted in Figure 2 and Table 1, under a shear wave, contact state alternates between 'stick' and 'slip'.

Table 1 Contact state alternation and critical time

Contact state	Slip → Stick	Stick → Slip	Slip → Stick	Stick → Slip
Critical time	$t_{c1} = t_c$	$t_{c2} = \frac{\pi}{\omega} - t_c$	$t_{c3} = \frac{\pi}{\omega} + t_c$	$t_{c4} = \frac{2\pi}{\omega} - t_c$

The shear stress variation caused by the ultrasonic wave is illustrated in Figure 2(a). When the contact sticks, the incident wave propagates through the interface without distortion. At a slipping contact, the maximum shear stress supported by the interface is the friction limit ($\mu\sigma$) and shear stress transmitted remains at that level. Figure 2(b) shows the wave distorted by slip at the interface.

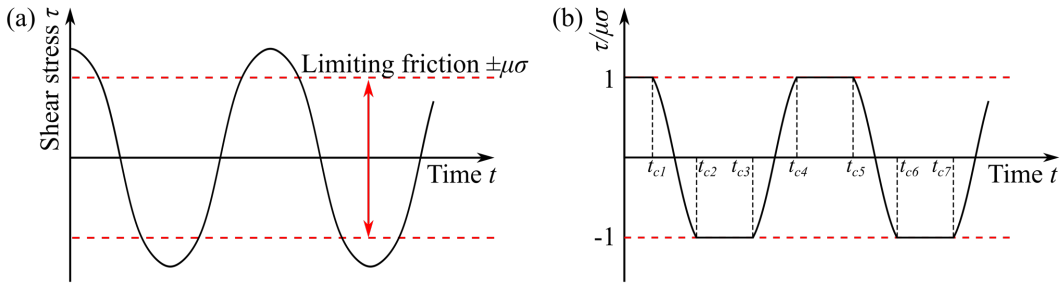

Figure 2 Shear stress caused by an ultrasonic wave and the effect of limiting friction at the interface: (a) before distortion; (b) after distortion.

Due to the truncation, the waveform in Figure 2(b) more closely resembles a square wave; which can be mathematically represented by $A = A_1 sin(\omega t) + A_3 sin(3\omega t) + A_5 sin(5\omega t) + \cdots$. The spectrum thus contains higher order odd harmonics (i.e. third ($3f$), fifth ($5f$), etc.) in the reflected and transmitted waves [17,20]. Detecting the presence of these higher orders, therefore, indicates that limiting friction has been exceeded and slip has occurred.

3 Mathematical Model

3.1 Governing equations

A mathematical modelling approach from [17, 23] is followed here (depicted in Figure 1). The incident shear wave and reflection in I and transmitted wave in II is described by $f(t - x/c)$, $g(t + x/c)$ and $h(t - x/c)$ respectively. Propagation of incident, reflected and transmitted waves are governed by the wave equation:

Deleted:

$$c^2 \frac{\partial^2 u(x,t)}{\partial x^2} = \frac{\partial^2 u(x,t)}{\partial t^2}, \tag{5}$$

where $u(x,t)$ is the displacement of the shear wave, c is the speed of sound in I and II. In each material, the total displacement is given by:

$$u^I(x,t) = f(t - x/c) + g(t + x/c), \tag{6}$$

$$u^{II}(x,t) = h(t - x/c). \tag{7}$$

The corresponding shear stress in I and II, τ is obtained as:

$$\tau^I(x,t) = G \frac{\partial u(x,t)}{\partial x} = \frac{G}{c}[-f'(t - x/c) + g'(t + x/c)], \tag{8}$$

$$\tau^{II}(x,t) = \frac{G}{c}[-h'(t - x/c)]. \tag{9}$$

The amplitude of the normal incident shear wave is assumed sufficiently large to trigger 'slip' at the interface. Constant contact stress, σ is applied to the interface to remain in a closed state during the alternation of 'stick' and 'slip' state. The boundary conditions are defined as:

$$\begin{cases} u^I = u^{II} + \Delta u \\ \tau^I = \tau^{II} \end{cases} \quad 'stick', \tag{10}$$

$$\tau^I = \tau^{II} = -sgn(\dot{u}^I)\mu\sigma \quad 'slip', \tag{11}$$

where Δu is displacement difference, $\dot{u}^I$ the total velocity at the interface in I and $sgn()$ the sign function. The friction is in the opposite direction to velocity at the interface (Equation (11)). Stress continuity at the interface regardless of contact state is described by $\tau^I = \tau^{II}$. Velocity at the interface is defined as:

Deleted:

$$\dot{u}^I(x,t) = \frac{\partial u^I}{\partial t} = f'(t - x/c) + g'(t + x/c). \tag{12}$$

Combined with Equation (8), expression of the derivative is given as:

Deleted:

$$\begin{cases} f'(t - x/c) = \frac{1}{2}\left(\dot{u}^I(x,t) - \frac{c}{G}\tau^I(x,t)\right), \\ g'(t + x/c) = \frac{1}{2}\left(\dot{u}^I(x,t) + \frac{c}{G}\tau^I(x,t)\right). \end{cases} \tag{13}$$

3.2 Numerical implementation

Several powerful tools have been developed for tackling stick-slip phenomena. 2-D Boundary Element Method (BEM) has been used in studying the interaction of out-of-plane shear wave [13] and in-plane waves [18] with the frictional interface. In recent work the Finite Element Method (FEM) has been used in modelling the nonlinear interaction of shear waves with a frictional interface and studied the contact nonlinear generation with normal incident shear wave [20] and oblique incidence [22] and incorporating roughness of the contact interface [24].

In this numerical study, the propagation of shear ultrasound and interaction at the frictional interface was modelled using a simplified 1-D finite difference (FD) model [21, 25]. Compared with other elaborate numerical and computational approaches, this simpler finite difference method is sufficient to capture the fundamental physical process, i.e. stick-slip phenomena at the interface, not the detailed modelling of practical situation. This simpler approach shows reasonable agreement with other methods for determining the effect of input amplitude and contact stress [21]. As illustrated in Figure 3, a half-space material and a rigid wall are in contact at $x = 0$ under a contact stress. A shear wave propagates from the source at $x = -L$ towards the interface. At $x = -L$, a transparent boundary is defined to permit waves only transmitting through towards $x = -\infty$.

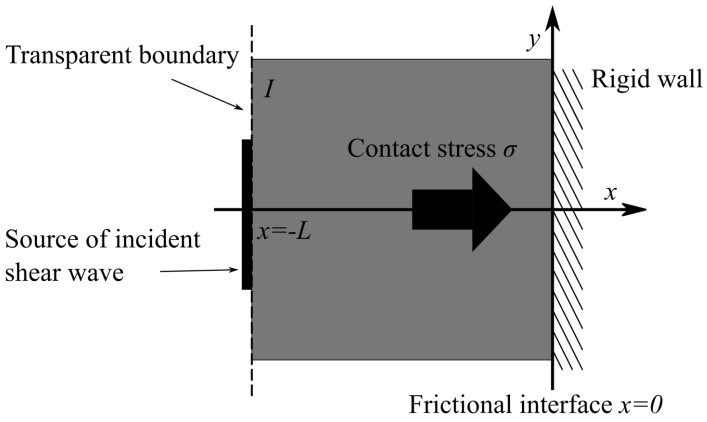

Figure 3 Schematic diagram of simplified 1-D model.

At the frictional interface, Equation (10)-(11) are rearranged as:

$$\begin{cases} |\tau^I(0,t)| < \mu\sigma \\ \dot{u}^I(0,t) = 0 \end{cases} \quad 'stick', \tag{14}$$

$$\begin{cases} |\tau^I(0,t)| = \mu\sigma \\ \tau^I(0,t)\dot{u}^I(0,t) \le 0 \end{cases} \quad 'slip'. \tag{15}$$

For simplicity, the static friction coefficient for 'stick' state in Equation (14) and the kinetic friction coefficient for 'slip' state in Equation (15) was assumed equal to a constant value μ. The wave equation (Equation (1)) is discretised using a classic Euler scheme as:

$$c^2 \frac{u_{i+1,j} - 2u_{i,j} + u_{i-1,j}}{\delta x^2} = \frac{u_{i,j+1} - 2u_{i,j} + u_{i,j-1}}{\delta t^2}, \tag{16}$$

where the subscript i and j denotes the space and time index, respectively. δx and δt are the space and time increment. The Courant-Friedrichs-Lewy (CFL) condition was considered and expressed as $c(\delta t/\delta x)$. This term should be less than unity to ensure a stable numerical solution. To resolve the third harmonic component, a fine space increment, less than a fiftieth of the wavelength of third harmonic was used. The CFL was approximately 0.7 in computation to ensure the stability.

At $x = -L$, to limit the computation domain size, a transparent boundary was used, defined by:

$$f'(t + L/c) = s(t) \tag{17}$$

where f' is defined in Equation (13) and $s(t)$ is the source term, equivalent to imposed particle velocity. At this boundary, incident wave defined by $s(t)$ enters the computational domain moving to the right and any backward wave is absorbed without further reflection.

After rearrangement, the strain formulation is obtained as Equation (18) and discretised as:

$$\frac{\dot{u}(-L,t)}{c} - \frac{\partial u(-L,t)}{\partial x} = \frac{2s(t)}{c}, \tag{18}$$

$$\frac{1}{2}\left(\frac{u_{1,j+1} - u_{1,j}}{\delta t} - c\frac{-3u_{1,j} + 4u_{2,j} + u_{3,j}}{2\delta x}\right) = s(t). \tag{19}$$

At the frictional boundary, $x = 0$, the contact was assumed 'stick' initially and the shear stress was obtained from the second-order upwind scheme discretisation. The next time step solution at this boundary is given by:

$$\begin{cases} \tau_{i,j} = G\dfrac{-3u_{i,j} - 4u_{i-1,j} + u_{i-2,j}}{2\delta x} \\ u_{i,j} = u_{i,j-1} \end{cases} \quad 'stick', \tag{20}$$

$$\begin{cases} \tau_{i,j} = \dfrac{2\delta x\tau_{i,j}/G + 4u_{i-1,j} - u_{i-2,j}}{2\delta x} \\ \tau_{i,j} = \pm\mu\sigma \end{cases} \quad 'slip'. \tag{21}$$

The procedure for computing the shear polarised ultrasound at a frictional interface is summarised in the flow chart Figure 4. This was coded in the MATLAB (MathWorks) environment and a single run, with a computation domain of 8890 nodes in time and 1500 spatial nodes, takes less than 1 second to execute on a conventional laptop.

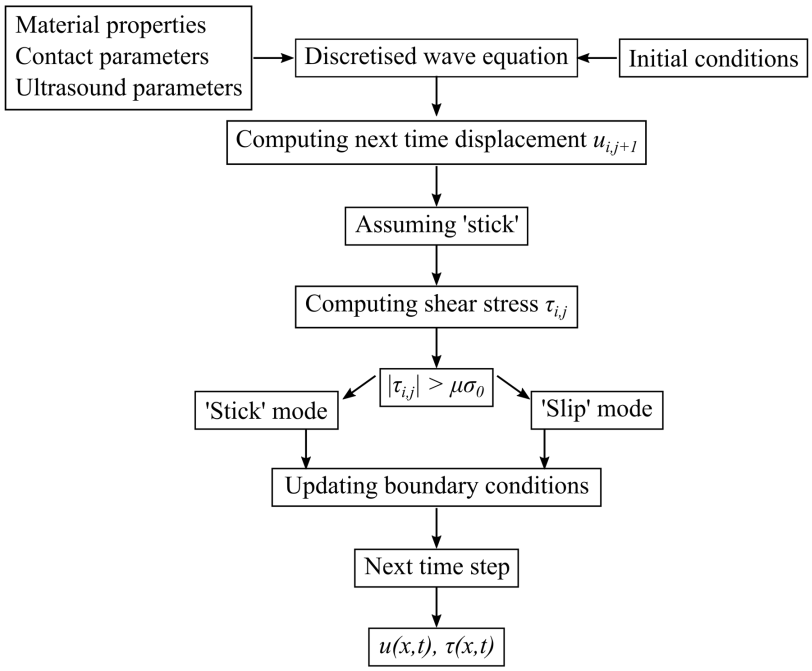

Figure 4 Flow chart of the numerical computation procedure.

3.3 Model results

A dimensionless parameter ξ has been used to assess the dependence of nonlinearity generation on ultrasound and contact parameters [17, 18, 20, 21]:

$$\xi = \frac{\mu\sigma}{GkA_0} \tag{22}$$

This dimensionless parameter defines the ratio of the friction limit to the maximum shear stress generated by ultrasound at the interface. For $0 < \xi < 1$ shear stress exceeds the limiting friction and 'stick-slip' motion occurs. A value greater than unity indicates the limiting friction is not exceeded and the contact remains in 'stick'.

$$\begin{cases} \xi = 0 & 'frictionless\ contact' \\ 0 < \xi < 1 & 'stick - slip' \\ \xi \geq 1 & 'stick' \end{cases}. \quad \textbf{(23)}$$

The energy carried by the ultrasound wave at a point x was calculated using the shear stress τ and the velocity $\dot{u}$ as:

$$E(x) = \int \tau(x,t)\dot{u}(x,t)dt. \quad \textbf{(24)}$$

The energy dissipation at the frictional interface was determined at $x = 0$. The energy and dissipation at the rough interface is shown in Figure 5. When contact is at 'stick' state ($\xi > 1$), no relative motion occurs at the frictional interface. Energy in the incident wave transfers into the transmitted wave and no energy is dissipated. During 'stick-slip', incident wave energy splits into reflected, transmitted waves and dissipation at the frictional interface. Most energy dissipates at $\xi \approx 0.4$. The total energy of reflection, transmission and the dissipation equals the total energy of the incident wave, which indicates energy conservation in the numerical model.

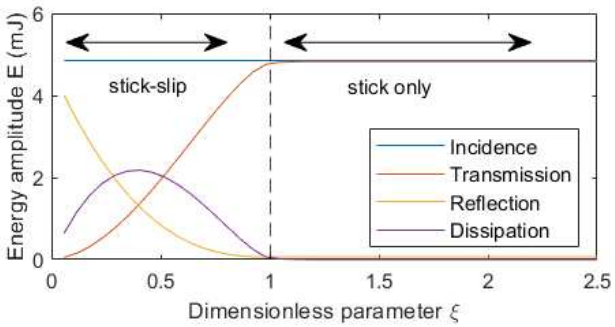

Figure 5 Energy carried by incident, reflected and transmitted wave and dissipation at frictional interface. (Friction coefficient 0.3 used).

The numerical computation was implemented in the time domain. The incident and the reflected signals were extracted from the time domain (Figure 6(a)) and a Fast Fourier Transform (FFT) was performed to yield the frequency spectrum (Figure 6(b)). The amplitude of both the fundamental frequency (f), A_1 and the third harmonic ($3f$), A_3 were determined.

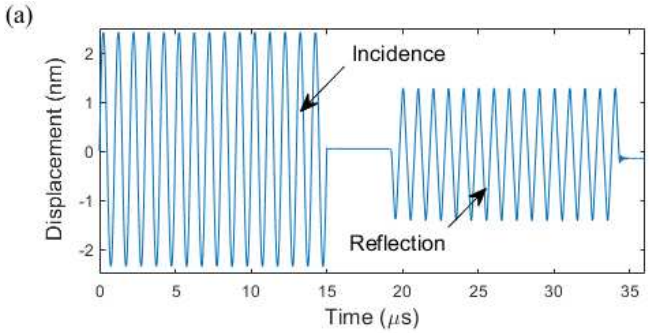

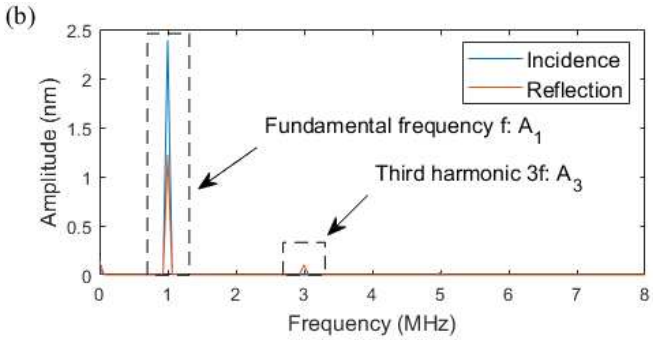

Figure 6 (a) Time domain and (b) frequency spectrum of incident and reflected wave numerically computed at x= -30mm. (For this case incident amplitude 2.4nm, contact stress 0.35MPa and friction coefficient 0.3 used).

The effect of the incident wave amplitude and the contact stress on harmonic generation was investigated using this numerical model. A stress range of 0 – 2 MPa was applied to compress the friction interface; this corresponds to the experiments performed (described in Section 4) where CAN was found to occur in this contact pressure range. The calculated amplitudes of the fundamental and third order harmonics are shown in Figure 7. Various levels of incident wave amplitude were simulated (1.6 - 6.4nm). As the contact was compressed, more shear wave energy travels through the interface and less reflects. So the fundamental frequency amplitude, A_1 decreases with increasing contact stress for the reflected wave (Figure 7(a)). A larger incident amplitude results in a larger reflected wave amplitude.

The third order harmonic amplitude, A_3 shows a characteristic 'rise-fall' shape with increasing contact stress, for all incident amplitudes (Figure 7(b)). At a low contact stress, the shear wave triggers 'slip-stick' motion and creates the nonlinear interaction. Increasing contact stress encourages nonlinearity generation and it peaks at $\xi = 0.5$ (as depicted in Figure 7(c)). Further compressing the contact, however, makes the ultrasonic shear stress difficult to overcome the increasing limiting friction. The 'stick-slip' is impeded and nonlinearity generation drops. Any further increase in the contact stress makes the contact fully 'stick' and no more nonlinear interaction occurs. A larger incident amplitude allows a higher contact stress at which the 'stick-slip' terminates (Figure 7(b)) and more harmonic generation.

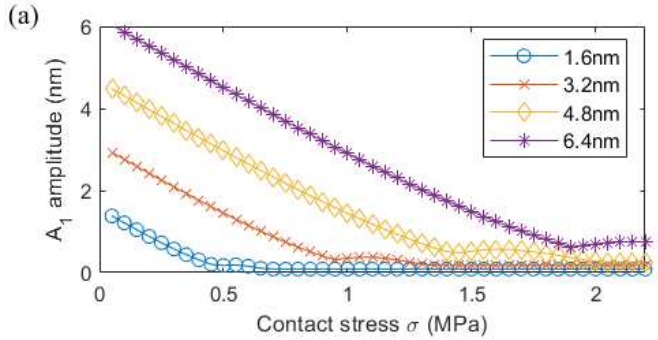

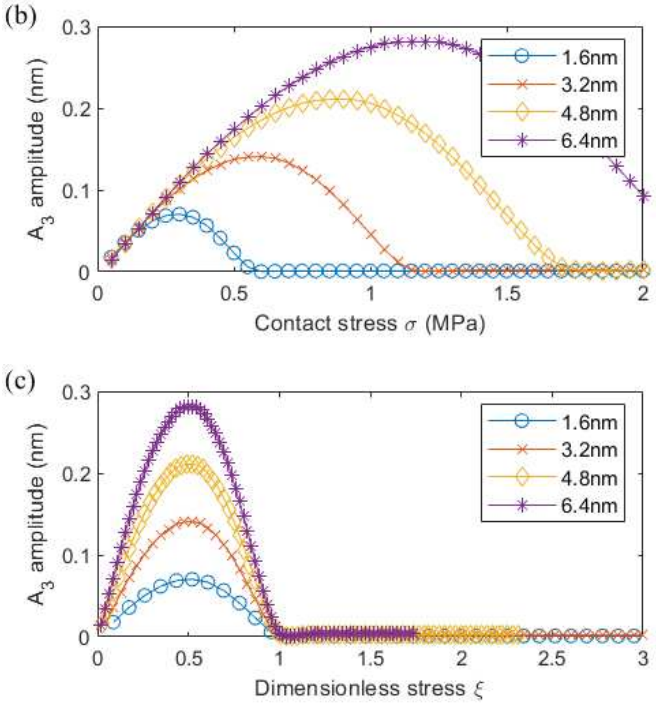

Figure 7 (a) Fundamental frequency amplitude, (b) third-order harmonic amplitude and (c) dimensionless stress. (For a friction coefficient of 0.3).

The effect of friction coefficient is shown in Figure 8. Increasing the friction coefficient makes harmonic generation occur over a narrower contact stress range. With a lower friction coefficient, the limiting friction is easy to overcome to permit the 'stick-slip' motion, even under high contact stress. With a higher friction coefficient, 'stick-slip' occurs only at low contact stress.

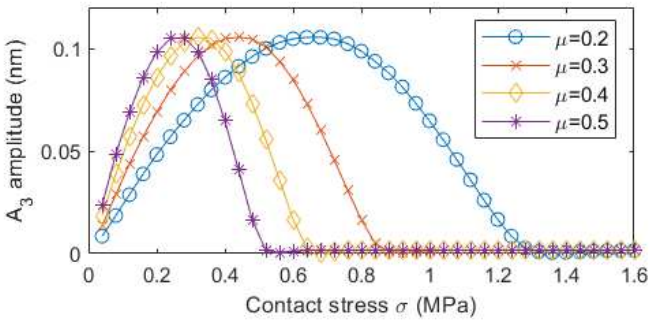

Figure 8 Effect of friction at interface on third-order harmonic amplitude.

4 Experiments

4.1 Loading apparatus and test specimens

Test specimens made from Aluminium Alloy 6082 were pressed together in a hydraulic loading frame, as shown in Figure 9. A load cell was placed on top of the specimen pair to measure the externally applied load. Specimens were first machined to a cylinder and then the contacting surfaces were ground and polished with abrasive papers of various grades. The surface roughness

of each test specimen was measured using an optical profilometer (InfiniteFocusSL, Alicona); the composite root mean square roughness of each specimen pair tested is given in Table 2.

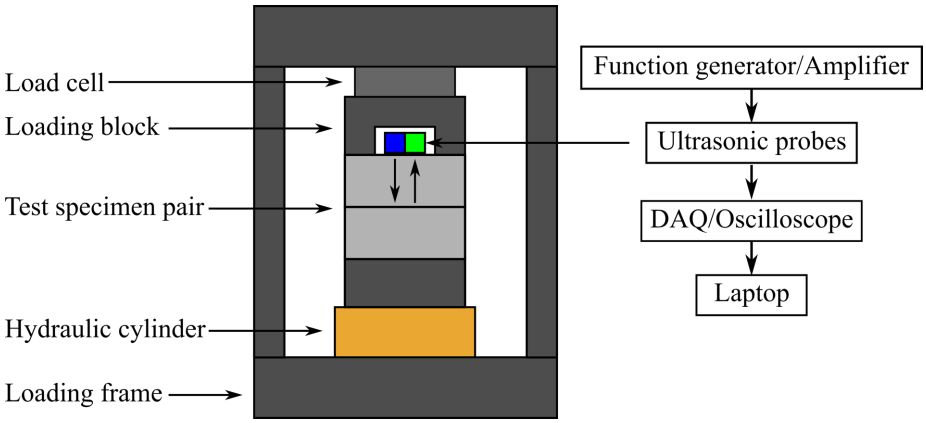

Figure 9 Schematic diagram of experimental setup and apparatus.

Table 2 Composite surface roughness of test contact pairs.

Contact pair #	1	2	3	4	5	6	7	8	9
Roughness (μm)	0.722	1.465	0.639	0.652	1.07	1.069	0.782	1.771	0.778

4.2 Instrumentation and transducers

The ultrasonic transmitter and receiver were clamped on the same side of the interface (Figure 9). The transmitter was a 1MHz normal incidence linear polarised shear wave ultrasonic transducer (V153, Olympus). The returning signal was received by a 5MHz wide-band shear wave ultrasonic probe (V155, Olympus). Piezoelectric elements (diameter of 12.7mm) were used as both transducers and the linear shear wave was generated. The transmitter works primarily at the fundamental frequency f and a wide-band ultrasonic transducer receives the returning signal, including both fundamental frequency f and the third harmonic component $3f$. This approach has been used in previous studies [15, 16, 21]. One practical advantage of this pitch-catch configuration over a transmission setup in [21] is that access is needed to only one side of the specimen pair, making the mechanical arrangement simpler. The other advantage is that in this experiment the nonlinear 'stick-slip' motion only occurs at low contact stress, where few asperities are in contact and the real area of contact is low; this results in a 'strong' reflection but a 'weak' transmission signal. In Figure 10, the reflected signal was measured with both a solid-solid interface and a solid-air interface.

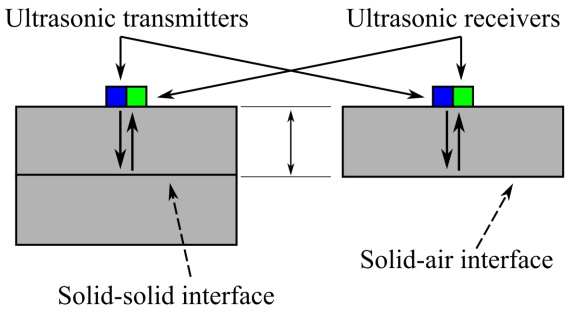

Figure 10 Configuration of the pitch-catch reflection method for the test case and a reference case.

Due to the thickness of the upper specimen, the path length of the 1MHz ultrasonic wave only permits approximately 20 cycles without overlapping with subsequent reflections. To maximise the interaction of shear wave with the frictional interface, a tone-burst 15-cycle sinusoidal wave was excited and amplified using a gated amplifier (RAM5000, Ritec) to drive the transmitter and the excitation voltage was from 2V to 560V (peak-peak). Received signals were digitised using an oscilloscope (Picoscope 5444B, Pico Tech) and stored on a laptop for post-processing.

4.3 Measurement of incident ultrasound shear stress

An important step in the analysis that follows is to know the magnitude of the shear stress generated at the interface by the incident ultrasonic wave. It is difficult to predict this on the basis of the magnitude of the voltage pulse used to drive the transmitter, as it depends on the piezo-electric constant and attenuation in the coupling layer and specimen material. In this work direct measurement of the displacement was carried out using a laser vibrometer (OFV534 and OFV 2500, Polytec) and converted to stress [21, 26].

It is challenging to measure the shear stress caused by ultrasound between test specimens as it lies in the plane of the contacting surface. Here, we measure the shear stress at a free (i.e. out of contact) surface and tacitly assume it is close to that when there is contact. The true displacement at contacting surface is overestimated, as displacement is greater at the free surface. This leads to the overestimation of shear stress. A 45° angle configuration was used (shown in Figure 11). The component of the shear wave displacement in x-direction was measured for the 1MHz ultrasonic transmitter which was exited at various voltages (90-560V). The measured displacement was converted to the displacement parallel to the contacting face along the tangential direction using simple trigonometry. The shear stress, τ induced by the ultrasound wave was then calculated from:

$$\tau = Gk\delta \tag{25}$$

where G is the shear modulus of specimen material, k is the wavenumber and δ is the displacement amplitude. The results for measured displacement and shear stress resulting from various excitation voltages are given in Table 3.

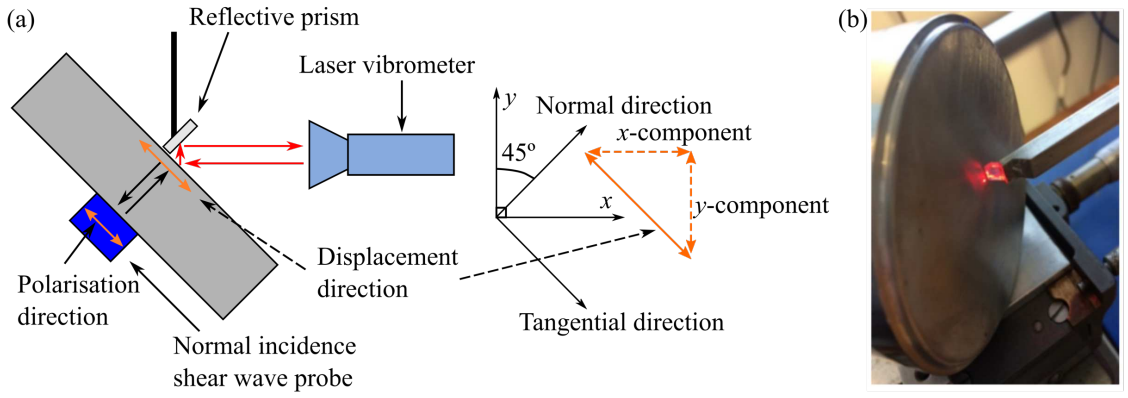

Figure 11 Configuration of surface shear stress measurement using a laser vibrometer.

Table 3 Measured displacements and shear stress at 1MHz caused by various voltages applied to the piezoelectric transducer.

Excitation voltage, V_{p-p}	90	140	280	420	560
Displacement, δ (nm)	9.13±2.83	14.52±1.39	21.97±1.76	31.37±1.78	42.35±1.41
Shear stress, τ (MPa)	0.50±0.15	0.79±0.08	1.19±0.10	1.71±0.10	2.30±0.08

4.4 Signal processing and removal of system nonlinearity

Figure 12(a) shows a raw captured waveform consisting of two successive reflections, as ultrasound bounced back and forth inside the specimen. Each reflection signal consisted of a 15-cycle sinusoidal waveform as the incident wave. A few steps were taken to process the signal. The first reflected signal was extracted from the time domain as its amplitude was maximum. A Hanning windowing function [26] was applied to the extracted signal and a Fast Fourier Transform (FFT) to obtain the frequency information and the amplitude of both the fundamental frequency, A_1 and the third harmonic, A_3 were recorded (Figure 12(b)).

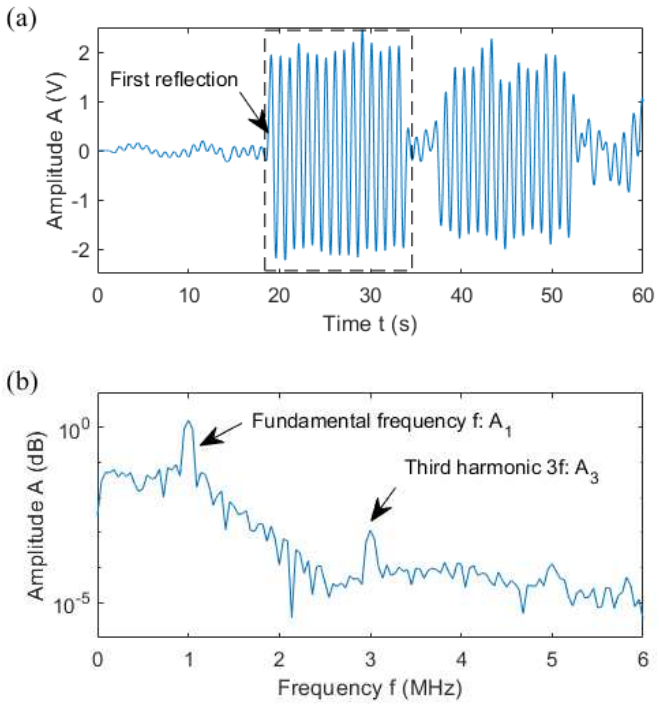

Figure 12 Steps in signal processing (a) extraction of the first reflected signal, (b) subsequent FFT (incident wave was a 15-cycle toneburst).

The frictional interface is not the only source of non-linearity in the reflected signal. The system will also be subject to in built non-linearities arising from, for example, the amplifier, coupling layer, or test specimen bulk materials. To remove these unwanted effects, an approach derived from [21] was used. A scaling factor C_a for the harmonic generation from a very low-power (excitation voltage 2V) solid-solid interface (Figure 10) (Equation (26)) and C_b for the nonlinearity from amplification in solid-air contact (Equation (27)) was derived to separate and

Deleted:

Deleted:

remove the nonlinear response originating inside the system from the measured nonlinearity (Equation (28)-(29)) to yield the nonlinearity only from the contact, A_3.

$$C_a = \frac{A_3^{m,L,ss}}{A_1^{m,L,ss}}, \tag{26}$$

$$C_b = \frac{A_3^{m,H,sa}}{A_3^{m,L,sa}}, \tag{27}$$

$$A_3^{s,ss} = C_a \times C_b \times A_1^{m,ss}, \tag{28}$$

$$A_3 = A_3^{m,ss} - A_3^{s,ss}. \tag{29}$$

where lowercase superscript s stands for system inbuilt nonlinearity, m for measured value, ss for solid-solid contact and sa for solid-air contact and upper case superscript L is for low power and H for high power conditions. Unless otherwise specified, A_3 refers to the nonlinearity from the contact in a solid-solid interface.

Figure 13 shows an example case for the measured harmonic $A_3^{m,ss}$, system inbuilt nonlinearity $A_3^{s,ss}$, nonlinearity from the contact A_3, as well as the measured harmonic from a solid-air interface, $A_3^{m,sa}$. The system inbuilt nonlinearity (i.e. from test equipment, test specimen and power supply) is less than the contact nonlinearity. The contact nonlinearity shows the characteristic 'rise-drop' shape with increasing contact stress. The system non-linearity, and the measured harmonic $A_3^{m,sa}$ for the solid-air interface do not vary with contact stress. This indicates that the 'stick-slip' at frictional interface is the cause of the nonlinearity generation. This approach has been adopted to remove system nonlinearity effects in the following experimental results.

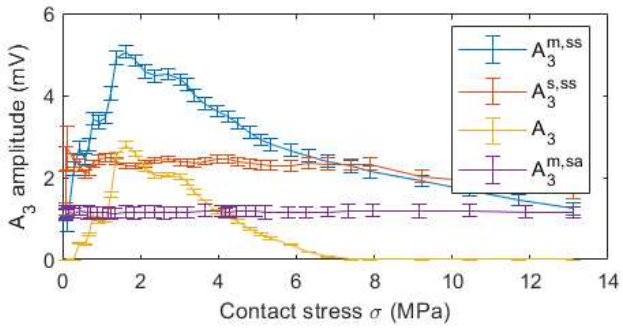

Figure 13 Measured harmonic $A_3^{m,ss}$, system inbuilt nonlinearity $A_3^{s,ss}$, nonlinearity from a solid-air interface $A_3^{m,sa}$, and extracted contact nonlinearity A_3 in a solid-solid contact (Input voltage 280V, Contact pair #1).

5 Experimental results

5.1 Measurement of contact non-linearity

Figure 14 shows the amplitude of the third harmonic A_3 from a solid-solid interface (contact pair #1) subject to various input voltages. The input voltage increases the amplitude of the ultrasonic wave and hence the shear stress at the interface. The 'rise-drop' characteristic is observed when the excitation was greater than 90V; from then on the magnitude of A_3 increased with increasing voltage.

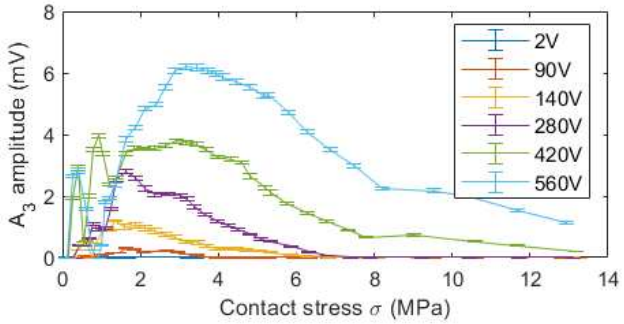

Figure 14 Measured amplitude of the third harmonic which indicates the amount of contact nonlinearity and hence slip (contact pair #1).

The effect of contact stress on contact nonlinearity generation is shown schematically in Figure 15. At low contact stress, there are only a few asperities in contact and real area of contact is low. The nonlinear 'stick-slip' phenomenon may just be triggered at those contact regions. Increasing contact stress at the interface brings more asperities into contact. There are therefore more asperity contacts subject to slip, more nonlinearity generation, and the amplitude of the third harmonic increases to a maximum. Further compressing the interface causes more contact to occur, but the shear stress ($\mu\sigma$) need to cause slip also increases. Less of the asperity contact points are able to slip and nonlinearity generation reduces. Eventually the contact stress is high enough such that no contact regions slip and nonlinearity generation falls to zero.

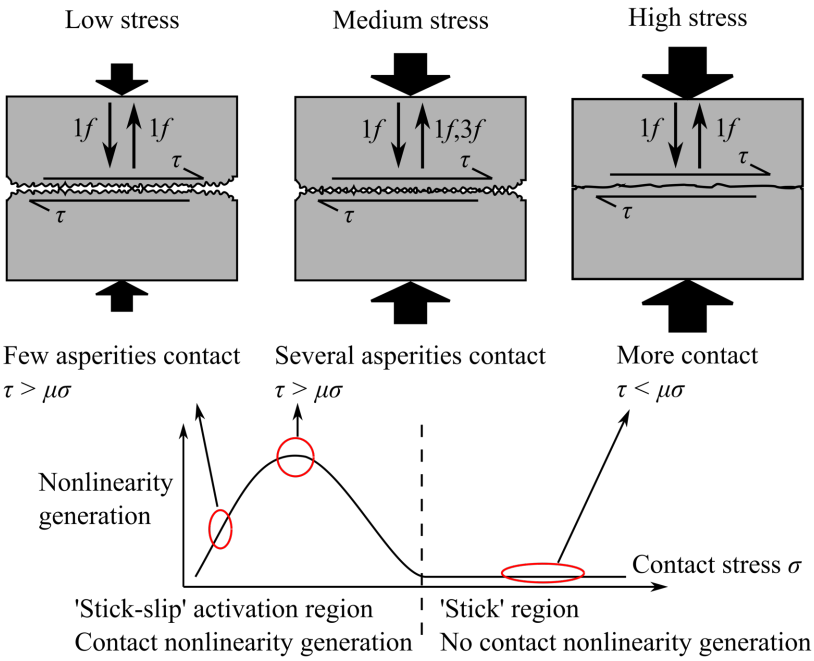

Figure 15 Schematic diagram of test specimens under various contact stress indicating regimes of nonlinearity generation.

5.2 Comparison with numerical results

The amplitude of contact nonlinearity A_3 measured in the experiment shown in Figure 14 is replotted as a contour map in Figure 16(a). The input voltages have been converted into shear stress using Equation (25) and the calibration data in Table 3 as described in Section 4.3. Figure 16(b) shows the prediction of the numerical model for the same parameter set. To facilitate the comparison with numerical computation, the harmonic amplitude A_3 has been normalised by dividing by the maximum contact nonlinearity measured.

Deleted:

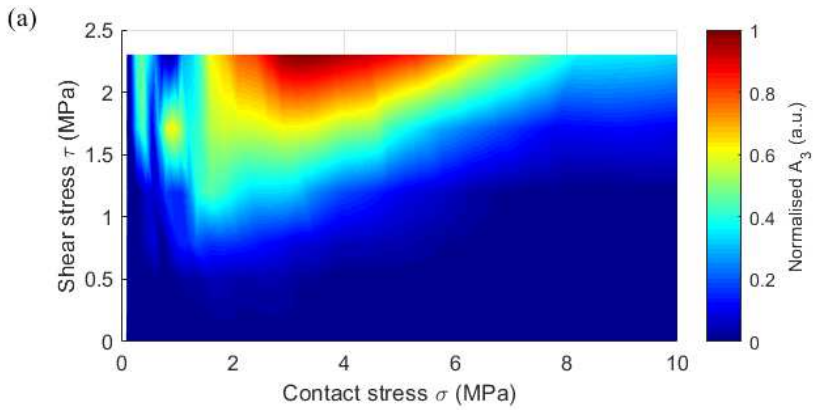

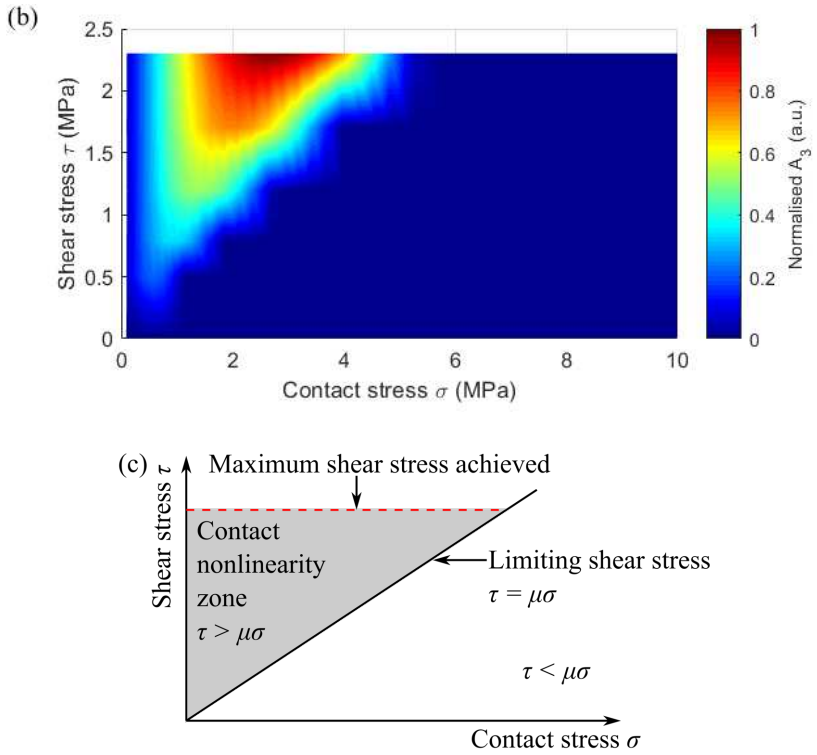

Figure 16 Comparison between (a) experimental and (b) numerical results for contact nonlinearity (friction coefficient of 0.42). (c) Schematic diagram of contact nonlinearity.

The region of nonlinearity where normal and shear stress are such that slip has occurred can clearly be seen in both plots, and the extent of nonlinearity generation resemble each other. In both experimental and numerical results, contact nonlinearity occurs at high shear stress (2.3MPa). Contact stresses in the range of (1.8-6.4MPa) in the experiment show significant generation of nonlinearity (shown by red contour, normalised value greater than 0.6), while in the numerical results, harmonic generation occurs at a narrower contact stress range (1.5-4.2MPa), which is mainly due to the effect of friction coefficient used in numerical computation.

Despite the friction coefficient difference used in this comparison, it may still be observed that experimental results offer smooth and gradual transition from contact nonlinearity generation (stick-slip zone) to non-generation (stick zone), while this transition is not clearly observed in the numerical results. Stick-slip and contact nonlinearity is stopped sharply in the numerical model with little transition. This sudden transition of limiting shear stress for slip to occur, is schematically shown in Figure 16(c).

The difference of transition from stick-slip zone to stick zone in experimental and numerical results is because the numerical model does not represent the contact of rough surfaces, demonstrated in Figure 17. In the simple 1-D FD model, only the dominant physical process, i.e. stick-slip phenomena is captured. In this model, contacting surfaces are assumed flat without realisation of asperities and the true contact area equals the apparent contact area. This means that the entire flat surface is in contact and slip occurs at all points in the contact simultaneously. In the experimental case, the contact is rough and occurs on a few load-bearing asperities where the nonlinear interaction takes places. Contact stress may not be evenly distributed. Elastic and plastic deformation may occur on these load-bearing asperities under high local normal stress and

this makes the contact in stick. Whilst the high normal stress, a few load-bearing asperities may develop into contact under low local stress, but high shear, which still makes slip occur. This has the effect of extending the nonlinear region to higher contact stress.

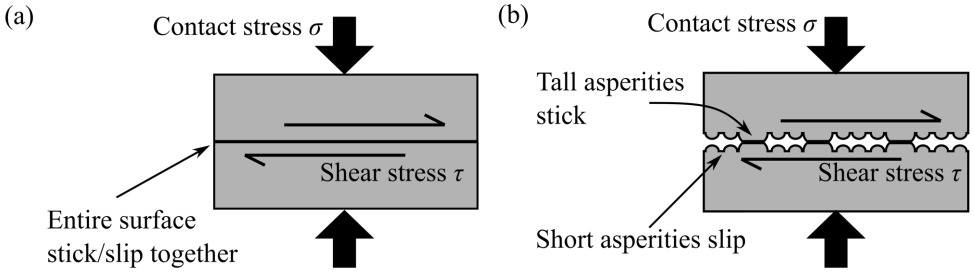

Figure 17 Contact conditions in (a) numerical and (b) experimental work.

5.3 Estimation of friction coefficient

In the previous section, experimental results show that the onset of slip can be observed from the appearance of contact nonlinearity in the reflected signal. In this section, two strategies have been used to calculate the friction coefficient from this nonlinear ultrasonic response.

5.3.1 Cut-off stress strategy

The first strategy was to use a 'cut-off' stress. The 'cut-off' stress is defined as the contact stress at which the harmonic generation no longer occurs. A clear 'cut-off' stress is easily observed in the numerical computation at $\xi = 1$ (Figure 18(a)). However, in the experimental data, it is more difficult to clearly identify this cut-off point (Figure 18(b)). Instead, it is easier to identify the corresponding contact stress at the nonlinearity peak ($\xi = 0.5$) and then to determine the 'cut-off' stress in the experimental results using $\sigma_{cut-off} = 2\sigma_{peak}$. The friction coefficient was then calculated using the 'cut-off' stress to divide the corresponding shear stress, τ according to $\mu = \tau/\sigma_{cut-off}$.

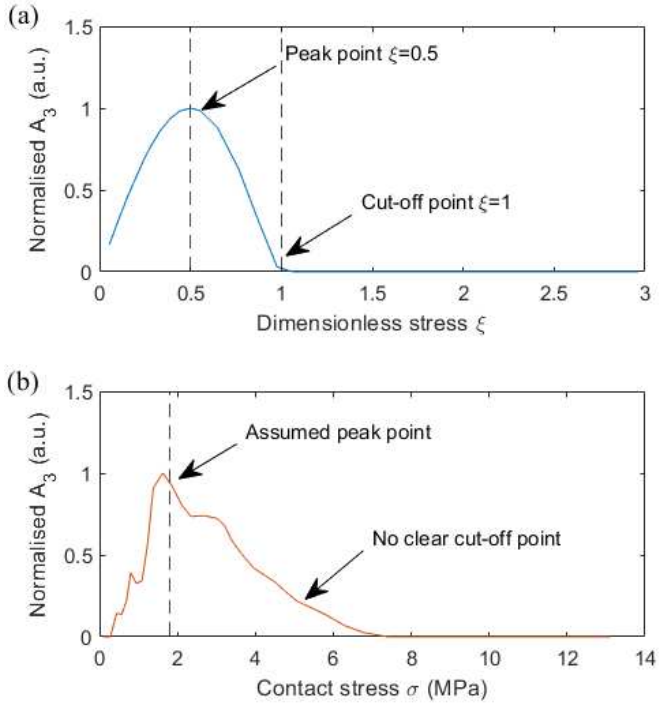

Figure 18 'Cut-off' stress and peak stress in (a) numerical computation and (b) experimental data (input 280V, contact pair #1).

This approach was applied to calculate friction coefficient at all the applied shear stresses for the test specimen pair. Peak points (above 0.98 of its maximum) of contact nonlinearity were selected (marked as '*') as shown in Figure 19. A fitting line was applied to these peaks and this shows an approximate linear relationship ($y = 0.588x$) between the shear stress and contact stress. For each incident shear wave, the gradient of the line through the origin and each peak point was calculated, and the approximate linear relationship between the shear stress and contact stress with averaged gradient is $y = 0.588x$. Half of this gradient was the estimated mean friction coefficient for all load cases, which is 0.294 (with standard deviation of 0.0712). The estimated cut-off line ($y = 0.294x$) is plotted on Figure 19(b) as dotted line.

In this cut-off stress approach, the cut-off stress however is estimated using the relationship ($\sigma_{cut-off} = 2\sigma_{peak}$) from the numerical study and assuming all contact surfaces are the same, which is ideal. In the experiment, the true cut-off stress in Figure 18(b) is approximately 7MPa, which is greater than twice the peak (approx. 2MPa). This may cause a friction coefficient over-estimated. The true cut-off stress varies between specimens.

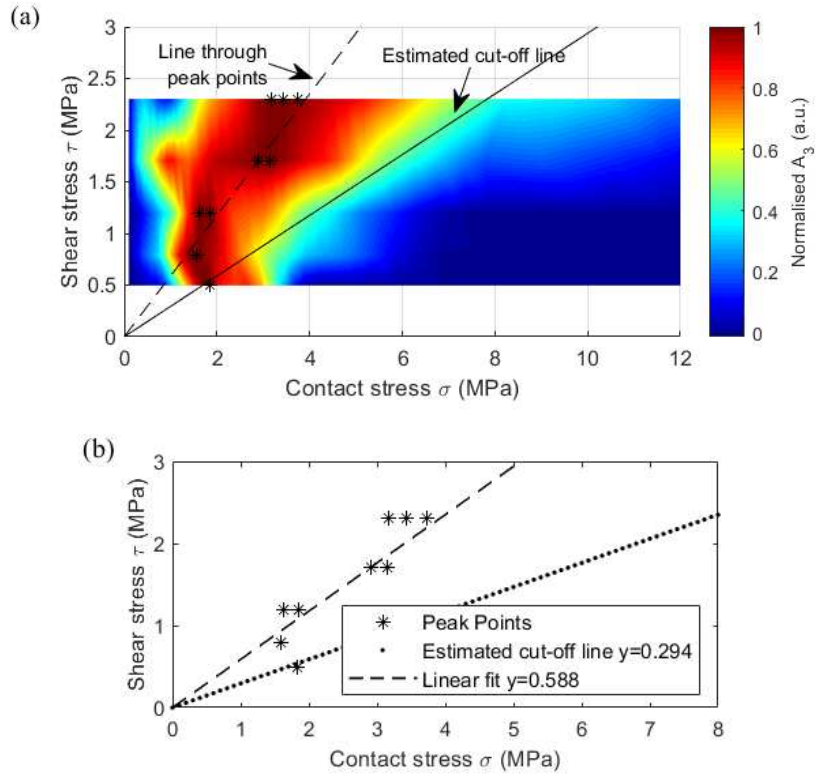

Figure 19 Friction coefficient estimation using 'cut-off' stress approach (contact pair #1).

5.3.2 Correlation strategy

In the second strategy, a simple correlation method was used to fit the numerical computation to experimental data. Experimental test condition of all loads (contact stress 0-14MPa and shear stress 0-2.3MPa) were used in the numerical model and friction coefficient was incrementally changed from 0 to 1 in steps of 0.01 in each computation. With each friction coefficient, the contact nonlinearity amplitude A_3 was first computed for test condition of all loads and then a correlation was carried out between the numerical results and the experimental data. The friction coefficient at which maximum correlation was achieved was recorded as the mean friction coefficient of all loads. Using this approach, the friction coefficient of the test specimen pair #1 was found approximately as 0.255 with a 98% bounds from 0.225 to 0.290 (Figure 20), which is used as the error of this approach.

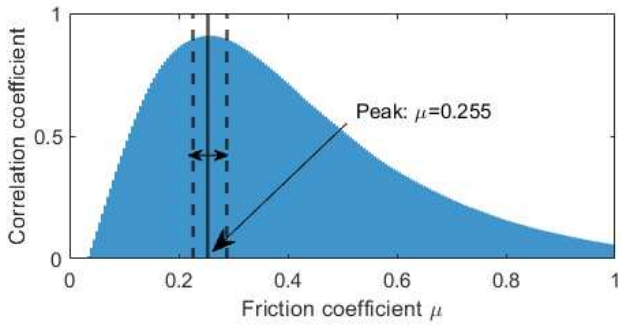

Figure 20 Friction coefficient estimation using correlation approach.

The correlation made between harmonic amplitude A_3 in the numerical and experimental work, depends on the performance of the numerical model. As this simple 1D model only captures the stick-slip process and nonlinearity generation, without further realisation at the interface, it affects the friction coefficient estimation.

5.3.3 Comparison of all friction coefficient values

Friction coefficient for all the contact pairs (Table 2) were measured using a simple sliding test configuration. In the sliding test, each actual test specimen pair was mounted on a tilting table. The table was tilted gradually until the top test specimen slid relative to the bottom one. The tilting angle was measured and converted into a friction coefficient.

The friction coefficients for each test contact pair, obtained using the two strategies described above, are shown in Figure 21. Results from the sliding test and published data [27] are shown for comparison. In published work, friction coefficient ranged from 1.2 to 1.4. In the sliding test for the contact pairs it ranged from 0.34 to 0.49, and the error was the standard deviation of 25 repeats. The friction coefficient estimated using cut-off stress and correlation strategies ranged from 0.22 to 0.61 and 0.22 to 0.54, respectively. The error of the cut-off stress method was obtained from the gradients calculated at the peak points of A_3. A 98% bounds was used as the error in the correlation approach.

The measurement using the ultrasonic method was carried out once for each contact pair. Repeats were not conducted since the contacting surfacing would differ after each contact loading-unloading process. During the measurement, a fixed shear stress was applied, and the contact stress was increased and removed, and then the next shear stress applied. For each loading condition (certain input shear stress and contact stress) 100 repetition was made. Due to the limited number of repeats in ultrasonic approach, this may increase the randomisation of the experiment.

Inevitably, it is not possible to reproduce test or environmental conditions precisely and so a degree of scatter is expected. Despite the variations, the friction coefficient measured using nonlinear ultrasound response is in broad agreement with the sliding test results.

The simple sliding test measures the friction coefficient when relative motion occurs between contact pairs. For the ultrasonic measurement the measured friction coefficient is from a localised micro-scale area, while the contact pairs remain static at macro scale. The environmental surface condition inevitably for these two methods will be different, this may cause the variation between results. The cut-off stress strategy uses the peak points (a low number of test conditions) while the correlation uses the entire set of test conditions. The friction coefficient from the correlation method has therefore more data than the cut-off stress approach which focuses only on the peak of contact nonlinearity; this may explain in part why the friction coefficient is greater in cut-off stress strategy for most contact pairs.

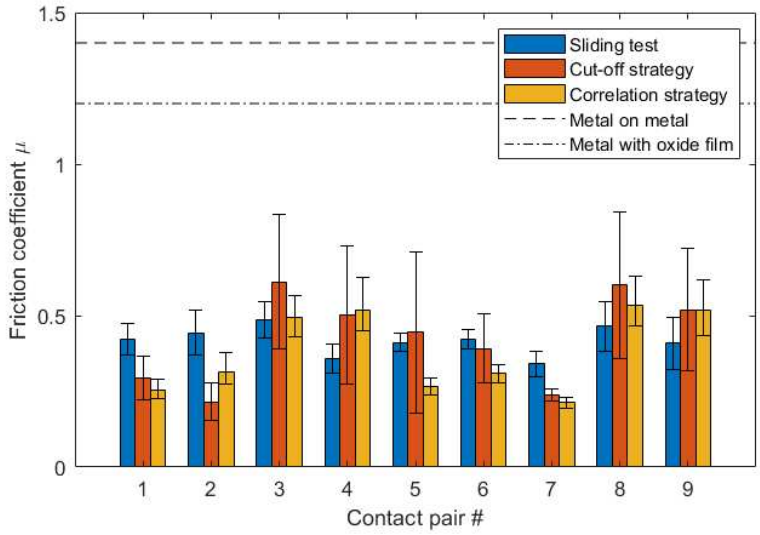

Figure 21 Friction coefficient measured using nonlinear ultrasonic approach (two strategies), sliding test, and from published data [27].

6 Discussion

The accurate measurement of coefficient of friction is challenging. The results are strongly affected by test method, environmental conditions and contacting surface conditions, which causes variations between measured friction coefficient. Nevertheless, the friction coefficient measured using the nonlinear ultrasonic response in-situ is comparable with published values. It is proposed that this ultrasonic method can be used to determine the friction coefficient of a contact interface in-situ.

However, there are some critical limitations to this approach. A fundamental limitation of the approach is the relatively low power, and hence shear stress, that can be generated with ultrasound. With the current measurement configuration, even when pulsing at 100's of volts, only low shear stress was achieved. This means the active contact stress range which allows the nonlinear 'stick-slip' motion is very limited (approximately less than 5MPa). This means that currently the approach would not be suitable to the high stress contact found in bearings or gear teeth. It is more likely to find application in lightly loaded, soft, or polymeric materials; provided these materials can transmit ultrasound without excessive attenuation. Increasing input shear stress can be achieved by further increasing excitation power, and also by increasing the effective sensor area. The generation of shear waves by mode conversion of an oblique incident longitudinal wave may also generate more powerful waves. However, all these approaches are likely to be rather ineffective compared to the increases in power likely to be required to overcome some 100's of MPa of contact pressure found in many practical machine elements.

Only dry contact was considered in this investigation. In practice, contact interfaces in machine components are lubricated. In a boundary lubrication where solid asperity contact is mixed with solid-lubricant contact, friction is the sum of solid-solid and solid-liquid parts. Stick-slip may still

occur at solid-solid contact and this may still cause generation of contact nonlinearity. For solid-lubricant part, nonlinearity of liquid may be measured and this could affect the measured harmonic and the friction coefficient estimation. Further work is needed for better understanding.

It is necessary to know the shear stress generated by the ultrasonic wave at the contact to estimate friction coefficient. A laser vibrometer was used to measure the displacement and stress of the incident ultrasound at the out-of-contact specimen surface. Analysis was then carried out under the assumption that the measured shear stress (from a solid-air interface) was equal to the true shear stress at the interface when in contact. This may lead to overestimation of ultrasonic induced shear stress and thence the friction coefficient. Further investigation is needed to access this assumption and understand the true shear stress in contact.

The 1-D model is a further limitation. Although the critical 'stick-slip' phenomenon and nonlinearity generation is captured using this simple model, due to the assumptions made, this approach is unable to represent the actual asperity contact at interface. In this research work only the static friction coefficient is considered and the kinetic friction coefficient is assumed to equal to the static friction coefficient. This may lead to some variations in the estimation of the friction coefficient. The estimation presents an 'averaged' friction coefficient at the contact.

In a sliding test friction coefficient is measured globally for contact pairs. In this ultrasonic method, although the ultrasonic sensor covers a relatively large area, the measurement is over a local region within the contact. This is a strength of this method as it offers the advantage of measuring friction coefficient locally in-situ, as friction may vary across an interface. However currently both ultrasonic approaches require many measurements at various loading conditions before an average friction coefficient is calculated, which is a weakness. This limits its application only in globally static conditions and impedes use in dynamic environment.

Finally, it is instructive to consider what is being measured in this kind of test, and what friction means at this scale. In a conventional test, specimens are slid past each other slowly, for a relatively long distance, and for just a few cycles (or maybe a few thousand). By contrast in this measurement method, the surfaces are slid past each other by only a few nanometres, extremely fast, and millions of times per second. What happens microscopically at this scale can only be the subject for speculation.

7 Conclusions

In this work a method to measure friction coefficient in-situ between two surfaces in nominally static contact has been developed. The approach uses the passage of a high-powered ultrasonic shear wave to cause a very small amount of slip at the interface. It proved possible to create shear stresses up to 2.3MPa at the interface which corresponded to surface deflections of around 40nm.

For lightly loaded contacts (up to 5MPa) it proved possible to record the effects of nonlinearity at the interface caused by slip taking place. The passage of an ultrasonic wave was modified by slip taking place causing the peaks of the wave to be truncated. The sinusoid then appears more like a square wave and so has higher order odd harmonics. The third order harmonic was recorded as a measure of nonlinearity and hence slip occurring.

The generation of nonlinearity was shown to rise to a peak and then fall as the contact stress on the specimen pair was increased from zero. At low contact stress there are few asperities in contact and so little slip taking place. As the stress rises the amount of slip incidents increases. This occurs until the shear stress no longer exceed its limiting value and the asperity sites begin to stick.

A simple one-dimensional numerical model was used to investigate this nonlinearity generation. The model was based on the solution of the wave equation for reflection at a boundary where slip was permitted at the interface. The same characteristic shape of nonlinearity generation was observed in the simulation.

Two different strategies were used to compare the experimental results with the model in order to estimate the friction coefficient. Friction coefficients in the range 0.22 to 0.61 were measured for a range of different roughness contact pairs. These were in broad agreement with published data and some simple sliding experiments.

Acknowledgements

The authors would like to acknowledge the financial support of the Engineering and Physical Sciences Research Council for funding this research through RDJ's fellowship on *Tribo-Acoustic Sensors* EP/N016483/1.

References

[1] Godfrey D. 1995 Friction oscillations with a pin-on-disc tribometer. *Tribol Int.* 28, 119–26. (doi:10.1016/0301-679X(95)92701-6)

[2] Ruan JA, Bhushan B. 1994 Atomic-scale friction measurements using friction force microscopy: part I—general principles and new measurement techniques. J. Tribol. 116, 378-388. (doi:10.1115/1.2927240)

[3] Ogletree DF, Carpick RW, Salmeron M. 1996 Calibration of frictional forces in atomic force microscopy. *Rev. Sci. Instrum.* 67, 3298–3306. (doi:10.1063/1.1147411)

[4] Schwarz UD, Köster P, Wiesendanger R. 1996 Quantitative analysis of lateral force microscopy experiments. *Rev. Sci. Instrum.* 67, 2560–2567. (doi:10.1063/1.1147214)

[5] Dunkin JE, Kim DE. 1996 Measurement of static friction coefficient between flat surfaces. Wear 193, 186-192. (doi:10.1016/0043-1648(95)06706-x)

[6] Sundararajan S, Bhushan B. 2001 Static friction and surface roughness studies of surface micromachined electrostatic micromotors using an atomic force/friction force microscope. *J. Vac. Sci. Technol. A.* 19, 1777–1785. (doi:10.1116/1.1353539)

[7] Blau PJ. 2001 The significance and use of the friction coefficient. *Tribol. Int.* 34, 585–591. (doi: 10.1016/S0301-679X(01)00050-0)

[8] Tronci G, Marshall MB. 2016 Understanding the behaviour of silver as a low friction coating in aerospace fasteners. *Tribol. Int.* 100, 162–170. (doi: /doi.org/10.1016/j.triboint.2015.12.050)

[9] Dwyer-Joyce RS, Harper P, Drinkwater BW. 2004 A method for the measurement of hydrodynamic oil films using ultrasonic reflection. Tribol. Lett. 17, 337-348. (doi:10.1023/B:TRIL.0000032472.64419.1f)

[10] Schirru MM, Sutton M, Dwyer-Joyce R, Smith O, Mills R. 2015 Development of a novel ultrasonic viscometer for real time and in-situ applications in engines. SAE Technical Papers 2015-1-0679.

[11] Chen W, Mills R, Dwyer-Joyce RS. 2018 Direct load monitoring of rolling bearing contacts using ultrasonic time of flight. Proc. R. Soc. A. 471:20150103. (doi:10.1098/rspa.2015.0103)
[12] Buck O, Morris WL, Richardson JM. 1978 Acoustic harmonic generation at unbonded interfaces and fatigue cracks. Appl. Phys. Lett. 33, 371-373. (doi:10.1063/1.90399)
[13] Mendelsohn DA, Doong JM. 1989 Transient dynamic elastic frictional contact: A general 2D boundary element formulation with examples of SH motion. Wave Motion 11, 1-21. (doi: 10.1016/0165-2125(89)90009-7)
[14] Barnard DJ, Dace GE, Rehbein DK, Buck O. 1997 Acoustic harmonic generation at diffusion bonds. J. Nondestruct Eval. 16, 77-89. (doi:10.1023/A:1022668417828)
[15] Biwa S, Hiraiwa S, Matsumoto E. 2006 Experimental and theoretical study of harmonic generation at contacting interface. Ultrasonics 44, 1319-1322. (doi: 10.1016/j.ultras.2006.05.010)
[16] Yan DW, Drinkwater BW, Neild SA. 2009 Measurement of the ultrasonic nonlinearity of kissing bonds in adhesive joints. NDT&E Int. 42, 459-466. (doi: 10.1016/j.ndteint.2009.02.002)
[17] O'Neill B, Maev RG, Severin F. 2001 Distortion of shear waves passing through a friction coupled interface. AIP Conference Proceedings 557, 1261-1267. (doi: 10.1063/1.1373899)
[18] Hirose S. 1994 2-D scattering by a crack with contact-boundary conditions. Wave Motion 19, 37-49. (doi: 0.1016/0165-2125(94)90011-6)
[19] Pecorari C. 2003 Nonlinear interaction of plane ultrasonic waves with an interface between rough surfaces in contact. J. Acoust. Soc. Am. 113, 3065-3072. (doi: 10.1121/1.1570437)
[20] Meziane A, Norris AN, Shuvalov AL. 2011 Nonlinear shear wave interaction at a frictional interface: energy dissipation and generation of harmonics. J. Acoust. Soc. Am. 130, 1820-1828. (doi:10.1121/1.3628663)
[21] Blanloeuil P, Croxford AJ, Meziane A. 2014 Numerical and experimental study of the nonlinear interaction between a shear wave and a frictional interface. J. Acoust. Soc. Am. 135, 1709-1716. (doi:10.1121/1.4868402)
[22] Blanloeuil P, Meziane A, Bacon C. 2014 Numerical study of nonlinear interaction between a crack and elastic waves under an oblique incidence. *Wave Motion* 51, 425–437. (doi:10.1016/j.wavemoti.2013.10.002)
[23] Richardson JM. 1979 Harmonic generation at an unbonded interface—I. planar interface between semi-infinite elastic media. Int. J. Eng. Sci. 17, 73-85. (doi: 10.1016/0020-7225(79)90008-9)
[24] Aleshin V, Delrue S, Trifonov A, Bou Matar O, Van Den Abeele K. 2018 Two dimensional modeling of elastic wave propagation in solids containing cracks with rough surfaces and friction – Part I: Theoretical background. *Ultrasonics* 82, 11–8. (doi.org/10.1016/j.ultras.2017.07.002)
[25] Blanloeuil P, Rose LRF, Veidt M, Wang CH. 2017 Time reversal invariance for a one-dimensional model of contact acoustic nonlinearity. J. Sound Vibr. 394, 515-526. (doi: 10.1016/j.jsv.2017.01.050)
[26] Liu SM, Croxford AJ, Neild SA, Zhou ZG. 2011 Effects of experimental variables on the nonlinear harmonic generation technique. IEEE Trans. Ultrason. Ferroelectr. Freq. Control 58, 1442-1451. (doi: 10.1109/TUFFC.2011.1963)
[27] Bowden FP, Tabor D. 2001 The friction and lubrication of solids. Oxford: Oxford University Press.